Beyond mean field description of shape coexistence in neutron-deficient Pb isotopes

R. R. Rodríguez-Guzmán
Institut für Theoretische Physik der Universität Tübingen, Auf der Morgenstelle 14, D-72076 Tübingen, Germany

J. L. Egido and L. M. Robledo
Departamento de Física Teórica C-XI, Universidad Autónoma de Madrid, 28049-Madrid, Spain
(Received 10 March 2004; published 26 May 2004)

The angular momentum projected generator coordinate method, with the axially symmetric quadrupole moment as generating coordinate, has been applied to study the shape coexistence and quadrupole collectivity in the neutron-deficient isotopes $^{182-192}$Pb. The finite range and density dependent Gogny interaction, with the parametrization D1S, has been used in the calculations. A good qualitative agreement with the available experimental results is found. Our results indicate that $Z=82$ remains, on the average, as a magic proton number for the considered nuclei and also support the experimental evidences for rotational bands built on coexisting low-lying states of oblate and prolate shapes.

DOI: 10.1103/PhysRevC.69.054319 PACS number(s): 21.60.Jz, 21.10.Re, 21.10.Ky, 21.10.Dr

I. INTRODUCTION

The low-lying states in neutron deficient lead isotopes have been studied theoretical and experimentally during the last three decades. The interest in this region is due to the presence of three 0^+ states within 1 MeV excitation energy in several even-even lead isotopes. The spherical 0^+ ground state is associated with the $Z=82$ magic number while the other two excited 0^+ are associated with prolate and oblate configurations based on particle-hole excitations. Nuclei around $Z=82$ exhibit a variety of coexisting configurations [1–14]. In particular, neutron-deficient Pb isotopes are spectacular examples of coexistence between oblate, spherical, and prolate low-lying 0^+ states. On the other hand, the recent discovery that the magicity of the $N=20$ and $N=28$ is more fragile than expected, see, for example, Ref. [15], has motivated the study of a possible erosion of proton shell closures. In this direction, recent studies [16–18] have provided valuable information about nuclei near $Z=82$ and have motivated an active investigation of the possible loss of magicity of this proton shell.

Experimentally, yrast and near-yrast states in the neutron-deficient Pb isotopes have been extensively studied using fusion-evaporation reactions. In the lighter isotopes ^{184,186,188}Pb around the neutron midshell nucleus ^{188}Pb, rotational bands have been observed in these experiments which were associated with prolate deformed shapes [2,19]. Crucial for the study of shape coexistence in these nuclei is the identification of excited 0^+ states some hundreds of keV above the ground state which is not possible in fusion-evaporation reactions. The first excited 0^+ states in $^{192-200}$Pb were identified in β-decay experiments using on-line isotope separators already fifteen years ago [6,12]. For the lighter isotopes, however, α decay becomes more and more probable relative to β decay and therefore α decay of Po isotopes combined with conversion electron spectroscopy to detect the E0 decays from the excited 0^+ states to the ground state is the ideal tool to study excited 0^+ states in ^{186,188,190}Pb. This type of experiments have recently been performed for all three isotopes mentioned above [3,4,20]. However, these experiments become more and more difficult when going to the lighter isotopes since the production cross sections for the Po isotopes in fusion-evaporation reactions are getting smaller (and the fission background larger) and at the same time, the α decay half-lives decrease down to milliseconds, complicating the separation process. Therefore, ^{186}Pb is so far the lightest Pb isotope for which two excited 0^+ states could be established.

The question if there were strongly deformed nuclei near $Z=82$ was already raised in Refs. [21,22]. At the mean field level there have been calculations using the Strutinsky method which have found low-lying deformed minima in Pb and Hg isotopes [23–25]. In Refs. [26–29] the relativistic mean field approximation was used to study shape coexistence in Pt, Hg, and Pb nuclei. The results of these studies were in contradiction with experimental data, especially the ones concerning deformed ground states in Pb and those of superdeformed ground states in Hg isotopes. The $Z=82$ shell closure in neutron-deficient Pb isotopes has been studied in Ref. [30] using both relativistic and nonrelativistic (Skyrme) mean field models and again deformed ground states were predicted. All these results clearly indicate that the standard relativistic mean field forces [31–34], and also some of the Skyrme forces, do not reproduce the ground state properties of at least some neutron-deficient nuclei in this region. Very recently [35], the new relativistic effective interaction NLSC has been introduced to describe ground state properties in Hg and Pb nuclei. Other Skyrme parametrizations [36–42]) also reproduce properly these states.

It is clear that a detailed description of the very rich structure of the energy landscapes in Pb and other nuclei of this region requires the inclusion of correlations beyond the mean field (see, for example, Refs. [36–42]). First, due to the presence of coexisting minima a configuration mixing calculation is called for. Second, symmetry restoration brings important topological changes in the corresponding mean field energy landscapes (see, for example, Ref. [41]). Furthermore, the states of the systems considered are probably the result of the subtle dynamical interplay between fluctuations in the collective parameters (mainly the quadrupole deformation) and the

zero point motion associated with the restoration of broken symmetries (mainly the rotational symmetry) and this interplay should be accounted for within a unified formalism.

The purpose of this paper is to perform a systematic study of the quadrupole collectivity in the neutron-deficient isotopes $^{182-192}$Pb. This set of nuclei is very challenging and attractive since, as mentioned, the experimental data [1–14] give evidences for strong shape coexistence between different low-lying configurations. Therefore, an accurate description of them, for different spin values, can be considered as a good testing ground for both effective forces and theoretical approximations. Besides this, we can also check the stability of the $Z=82$ proton shell closure, both at the mean field level and beyond, under extreme conditions associated with a very neutron-deficient regime. In the present study both configuration mixing and angular momentum projection are taken into account in the framework of the angular momentum projected generator coordinate method (AMPGCM) [43]. We have used in our calculations the Gogny interaction [44] with the parametrization D1S [45]. As it has been shown, this force is not only well suited to provide reasonable results for many nuclear properties all over the nuclear chart, but also to supply a good description of the phenomenology of the quadrupole collectivity in the regions $N\approx 20$ [43,46–52] and $N\approx 28$ [48,49] within a free parameter framework similar to the one used in the present paper. The quadrupole collectivity around $Z\approx 82$ has been previously considered with the Gogny force in the framework of the collective Hamiltonian [39], within the GCM [40] without angular momentum projection, and also at the mean field level [54].

The paper is organized as follows. In Sec. II we briefly describe the theoretical formalism used in this study. This formalism is the AMPGCM [43,47,48,50–52] with the axially symmetric quadrupole moment as generating coordinate. The results of our mean field, angular momentum projection (AMP) and configuration mixing calculations (AMPGCM) for the isotopes $^{182-192}$Pb are discussed in different subsections of Sec. III. Finally, Sec. IV is devoted to some concluding remarks.

II. THEORETICAL FRAMEWORK

As in previous works [43,47,48,50–52], we have used a mean field based procedure where the underlying mean field is determined first and then additional correlations are included through the AMPGCM with the mass quadrupole moment as generating coordinate. We have restricted ourselves to axially symmetric configurations and used the following ansatz for the $K=0$ AMPGCM wave functions:

$$|\Phi^I_\sigma\rangle = \int dq_{20} f^I_\sigma(q_{20}) \hat{P}^I_{00} |\varphi(q_{20})\rangle, \tag{1}$$

where $\hat{P}^I_{00}$ is the angular momentum projector operator restricted to $K=0$ states. The set of intrinsic wave functions $|\varphi(q_{20})\rangle$ was generated by solving the full Hartree-Fock-Bogoliubov (HFB) equations constrained to the desired mass quadrupole moment $q_{20}=\langle Q_{20}\rangle=\langle\varphi(q_{20})|z^2-1/2(x^2+y^2)|\varphi(q_{20})\rangle$. The quasiparticle operators associated with each intrinsic state $|\varphi(q_{20})\rangle$ were expanded in an axially symmetric harmonic oscillator (HO) basis containing thirteen major shells and the two length parameters of the basis $b_\perp$ and b_z were chosen to be always equal to keep the basis closed under rotations [53,55] (this is also the reason to include full HO major shells in the basis). The same oscillator length was used for all the quadrupole deformations considered in order to avoid completeness problems in the configuration mixing calculations [55].

The amplitudes $f^I_\sigma(q_{20})$ as well as the energies E^I_σ of the AMPGCM states $|\Phi^I_\sigma\rangle$ are obtained through the solution of the Hill-Wheeler (HW) equation

$$\int dq'_{20} \mathcal{H}^I(q_{20},q'_{20}) f^I_\sigma(q'_{20}) = E^I_\sigma \int dq'_{20} \mathcal{N}^I(q_{20},q'_{20}) f^I_\sigma(q'_{20}), \tag{2}$$

which is given in terms of the projected norm

$$\mathcal{N}^I(q_{20},q'_{20}) = \langle\varphi(q_{20})|\hat{P}^I_{00}|\varphi(q'_{20})\rangle \tag{3}$$

and the projected Hamiltonian kernel

$$\mathcal{H}^I(q_{20},q'_{20}) = \langle\varphi(q_{20})|\hat{H}\hat{P}^I_{00}|\varphi(q'_{20})\rangle. \tag{4}$$

To account for the fact that the mean value of the particle's number operator usually differs from the nucleus' proton and neutron numbers, we followed the usual recipe (see, for example, Refs. [56,57]) and replaced in Eq. (4) the operator $\hat{H}$ by $\hat{H}-\lambda_Z(\hat{Z}-Z_0)-\lambda_N(\hat{N}-N_0)$ where λ_Z and λ_N are average chemical potentials for protons and neutrons, respectively. The averaging procedure is performed among all chemical potentials $\lambda(q_{20})$, see Ref. [57] for further details.

As the functions $f^I_\sigma(q_{20})$ cannot be interpreted as probability amplitudes, we introduced the collective wave functions

$$g^I_\sigma(q_{20}) = \int dq'_{20}\, f^I_\sigma(q'_{20}) (\mathcal{N}^{1/2})^{I*}(q_{20},q'_{20}), \tag{5}$$

which are orthonormal and their module squared has, therefore, the meaning of a probability.

The $B(E2)$ transition probabilities and the spectroscopic quadrupole moments $Q^{spec}(I,\sigma)(I\geqslant 2)$ are given by

$$B(E2,I_i\to I_f) = \frac{e^2}{2I_i+1}\left| \int dq_{20} dq'_{20} f^{I_f*}_{\sigma_f}(q'_{20}) \times \langle I_f q'_{20}\|\hat{Q}_2\|I_i q_{20}\rangle f^{I_i}_{\sigma_i}(q_{20}) \right|^2, \tag{6}$$

$$Q^{spec}(I,\sigma) = e\sqrt{\frac{16\pi}{5}} \begin{pmatrix} I & 2 & I \\ I & 0 & -I \end{pmatrix} \int dq_{20} dq'_{20} f^{I,\sigma*}(q'_{20}) \times \langle I q'_{20}\|\hat{Q}_2\|I q_{20}\rangle f^{I,\sigma}(q_{20}) \tag{7}$$

with

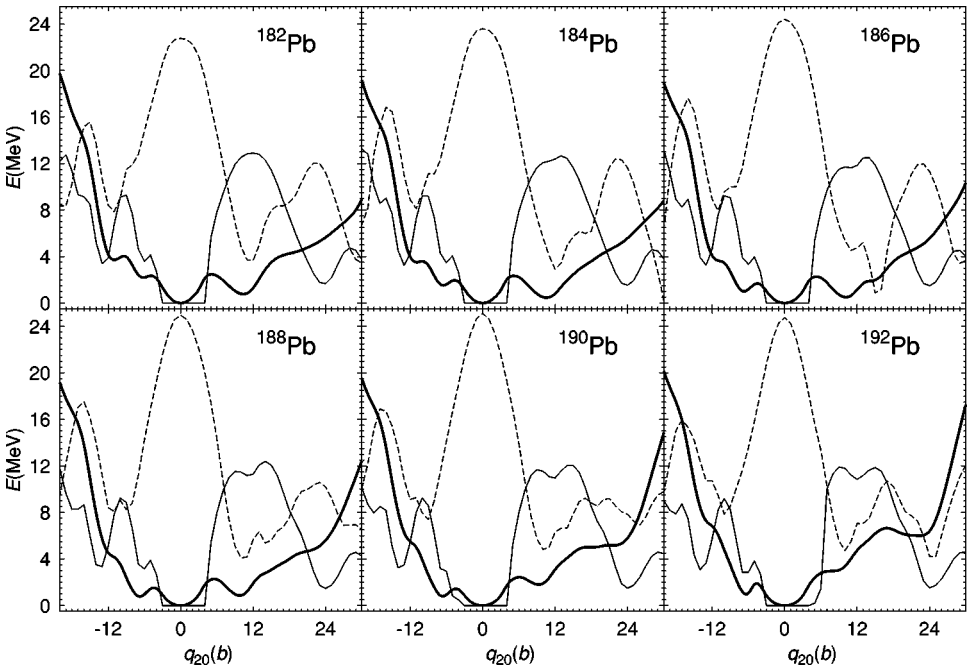

FIG. 1. Mean field potential energy surfaces (continuous thick line) as well as the absolute value of the pairing energies for neutrons (dashed line) and protons (continuous thin line) for the nuclei $^{182-192}$Pb considered as functions of the axially symmetric quadrupole moment. The energy scale is the same for all curves.

$$\frac{\langle I_f q'_{20}\|\hat{Q}_2\|I_i q_{20}\rangle}{(2I_i+1)(2I_f+1)} = \sum_{\mu} \begin{pmatrix} I_i & 2 & I_f \\ -\mu & \mu & 0 \end{pmatrix} \int_0^{\pi/2} d\beta \sin\beta d^{I_i}_{-\mu,0}(\beta) \times \langle \varphi(q'_{20})|\hat{Q}_{2\mu} e^{-i\beta \hat{J}_y}|\varphi(q_{20})\rangle,$$

where the indices i and f stand for the initial and final states and $\hat{Q}_{2\mu}$ are the charge quadrupole moment operators. As we are using a large, no core configuration space no effective charges are needed. Further details on the computational procedure can be found in Ref. [43].

III. RESULTS

This section presents the results of our calculations. Since the mean field approximation is our starting point, it will be discussed first in Sec. III A. Calculations beyond the mean field are considered in Sec. III B to consider the effect of the angular momentum projection. In Sec. III C the effect of configuration mixing and angular momentum projection is discussed. Partial results for some lead isotopes at the mean field level [41] and within the GCM approach [40] (but without angular momentum projection) have been already discussed elsewhere, therefore, in the corresponding subsections we shall just concentrate on the discussion on aspects and nuclei either not discussed before or relevant for the understanding of the AMPGCM approximation.

A. Mean field approximation (MFA)

The results of the q_{20}-constrained HFB calculations are displayed in Fig. 1, where we show (thick lines) the mean field potential energy surfaces (MFPES) for the isotopes $^{182-192}$Pb as functions of the axially symmetric quadrupole moment q_{20}. All these nuclei have spherical ground states, as a clear indication of the strong signature of the $Z=82$ proton shell closure at the mean field level. On the other hand, several oblate and prolate competing minima appear at very low energy, reflecting a pronounced shape coexistence. The first 0^+ excited states in the light isotopes $^{182-186}$Pb are prolate and the second ones oblate with deformation parameters $\beta_2=0.29$, 0.32, and 0.29 ($\beta_2=-0.18$, -0.18, and -0.20), respectively. In $^{188-192}$Pb, the situation is reversed: the first excited states are oblate with deformation parameters $\beta_2=-0.20$, -0.20, and -0.17 while the second ones are prolate with $\beta_2=0.28$, 0.25, and 0.22, respectively. The spherical, oblate, and prolate states are practically orthogonal, the largest norm overlap is 0.0066, corresponding to the spherical and oblate states of the nucleus ^{188}Pb. This orthogonality guarantees that the energies of these states can be used to calculate excitation energies. Experimentally the shape change of the first and second excited states takes place in ^{186}Pb, two mass units earlier than in our calculations. The excitation energies of the three minima as well as their quadrupole moments are given in columns 3 and 4 of Table I. The agreement with the experimental results [1–14], shown in the first column of the same table, is very good if one takes into account that no additional fitting of the interaction has taken place.

In Fig. 1 the proton and neutron pairing energies are also shown. As expected, the proton pairing energies vanish at and around the spherical shape because of the $Z=82$ shell closure. The neutrons, on the contrary, display very large pairing energies around these shapes. These results explain the fact that two quasiparticle states are not found at energies below the collective prolate or oblate minima. At larger q_{20} values the neutron pairing energies decrease very sharply while the proton ones rise at the same extend. Neither the proton nor the neutron pairing energies change very much with the mass number. Other mean field quantities, like single particle energies, for example, can be found in Ref. [41].

Though our HFB results provide a reasonable description of the known excitation energies for the 0^+ states in these

TABLE I. Excitation energies and intrinsic quadrupole moments of 0^+ excited states in $^{182-192}$Pb. The quadrupole moment is defined as $q=\langle Q_{20}\rangle$. The quadrupole moments of the 0^+ excited states are not known experimentally. States designated as oblate (prolate) in experimental papers are put on the oblate (prolate) line.

	Experiment	MFA		AMP		AMPGCM		GCM	
Nucleus	E(MeV)	E(MeV)	$q(b)$	E(MeV)	$q(b)$	E(MeV)	$q(b)$	E(MeV)	$q(b)$
^{182}Pb	0.000	0.000	0.0	0.0		0.00	0.22	0.0	0.00
	0.817	0.788	10	0.761	11	1.13	10.45	0.970	10.6
		2.20	−6	2.23	−7	2.50	−5.93	1.78	−0.22
^{184}Pb	0.000	0.000	0.0	1.4		0.00	0.22	0.0	0.00
	0.610	0.490	11	0.421	11	0.850	10.74	0.68	10.3
		1.60	−6	1.52	−7	1.90	−5.50	1.61	−3.6
^{186}Pb	0.000	0.000	0.0	0.0		0.00	0.23	0.0	0.0
	0.532	1.04	−7	1.03	−7	1.44	−6.46	1.28	−6.2
	0.600	0.512	10	0.538	11	0.89	10.30	0.79	10.0
^{188}Pb	0.000	0.000	0.0	0.0		0.00	0.15	0.0	0.0
	0.600	0.787	−7	0.802	−7	1.25	−2.60	1.04	−6.4
	0.710	0.871	10	0.876	10	1.33	5.95	1.15	9.23
^{190}Pb	0.000	0.000	0.00	0.0		0.00	0.12	0.00	0.00
	0.658	0.861	−7	0.810	−7	1.31	−6.09	1.12	−6.3
	1.020	1.81	9	1.71	10	2.12	8.77	1.67	0.4
^{192}Pb	0.000	0.000	0.0	0.0		0.00	0.32	0.0	0.00
	0.77	1.04	−6	1.01	−7	1.29	−6.56	1.34	−5.15
		2.96	8	2.86	9	2.79	6.49	1.69	−1.03

nuclei, this raw mean field approximation can only be considered as zero order treatment because additional correlations may modify the results already described. Because of the very pronounced shape coexistence it is really difficult to assert *beforehand* to which extent this will happen.

B. Correlations beyond the mean field: Angular momentum projection

Before considering the full AMPGCM it is instructive to look into the angular momentum projected potential energy surfaces (AMPPES) defined as

$$E^I(q_{20}) = \frac{\mathcal{H}^I(q_{20},q_{20})}{\mathcal{N}^I(q_{20},q_{20})}. \tag{8}$$

These quantities are the diagonal terms of the AMPGCM matrix and provide very useful information because it gives the energy gained by angular momentum projection as a function of the quadrupole moment. This energy is in many cases the most important part of the interaction and whenever the AMPPES shows a well pronounced minimum the probability distribution [Eq. (5)] concentrates around it. In Fig. 2, the quantities $E^I(q_{20})$ are plotted for the nuclei $^{182-192}$Pb and $I^\pi=0^+$, 2^+, 4^+, 6^+, and 8^+. For details about the omitted points around $q_{20}=0$ see Ref. [43]. The corresponding MFPES (dashed lines) are also included for comparison.

In the MFA we observe that with decreasing neutron number, i.e., as we approach the drip line, the PES's get wider. It is interesting to observe that the effect of the AMP is to reinforce this tendency, i.e., the projected PES are broader than the MFA ones. For $I^\pi=0^+$ the general behavior of the projected surfaces is rather similar in all isotopes. At $q_{20}=0$, as expected, one does not obtain any rotational energy correction to the spherical mean field. At approximately −3 b and +3 b, two nearly degenerate (the energy differences between them are 59, 67, 64, 60, 63, and 67 keV for $^{182-192}$Pb) minima appear. The origin of these two peaks can be traced back to the peculiar behavior with q_{20} of the matrix elements $\langle\varphi(q_{20})|HJ_y^2|\varphi(q_{20})\rangle$ and $\langle\varphi(q_{20})|J_y^2|\varphi(q_{20})\rangle$ for closed shell nuclei, see Ref. [58]. These matrix elements enter in the semiclassical expression of the rotational energy correction. The minima at ±3 b are separated by the spherical barrier which is around 3 MeV in all cases. As we will see later on, these two additional AMP minima, though bringing such a significant topological change with respect to the MFPES, do not provide new physical configurations because they average to produce a highly correlated spherical ground state. For quadrupole moments with absolute values larger than 3 b the AMPPES look rather similar to the MFPES, but shifted, on the average about 4 MeV. The main characteristic of the MFPES, i.e., the coexisting prolate and oblate minima, is maintained by the AMPPES. The excitation energies of these AMP prolate and oblate 0^+ minima as well as their quadrupole moments are displayed in columns 5 and 6 of Table I. Concerning the quadrupole moment of the lowest 0^+, we do not quote any value because there are two almost degenerate minima at ±3 b. We observe that the AMP excitation energies (and also the q_{20} intrinsic deformations) are very similar to the mean field results. Notice that the energy difference $E(0_3^+)-E(0_2^+)$ is independent of the origin of energies, i.e.,

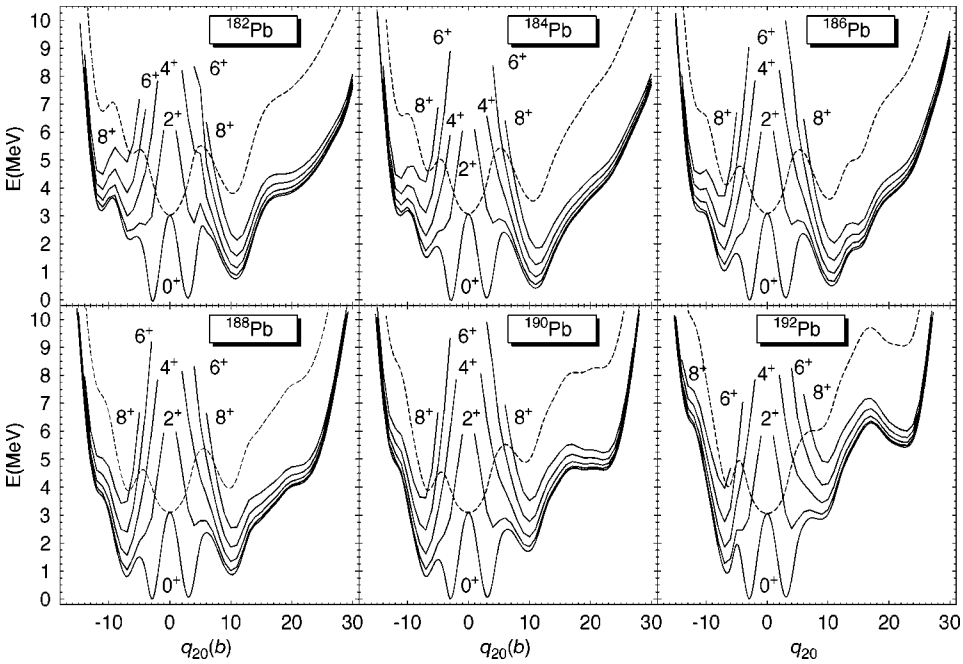

FIG. 2. Angular momentum projected potential energy surfaces (full lines) for the nuclei $^{182-192}$Pb and for the spin values $I^{\pi}=0^{+},2^{+},4^{+},6^{+}$, and 8^{+}, plotted as a function of the axially symmetric quadrupole moment q_{20}. The mean field potential energy surfaces (dashed lines) are also plotted for comparison. In each nucleus, the energies are referred to the $I^{\pi}=0^{+}$ ground state.

independent of our choice of $E(0_1^+)$, and it also agrees very well with the corresponding difference in the MFA.

For $I^{\pi}=2^{+}$, 4^{+}, 6^{+}, and 8^{+}, the lowest energy deformed minima of the AMPPES in $^{182-186}$Pb are prolate with intrinsic deformations of 11 b. In ^{188}Pb we observe a very strong competition between the oblate minimum at −7 b and the prolate ground state at 10 b for $I^{\pi}=2^{+}$, the energy difference amounts only to 16 keV. This shape coexistence is also present for the spin values $I^{\pi}=4^{+}$ and $I^{\pi}=6^{+}$ for which the energy differences are 224 and 540 keV, respectively. The corresponding energy difference reaches 872 keV for $I^{\pi}=8^{+}$. In ^{190}Pb for the spin values $I^{\pi}=2^{+},4^{+}$, and 6^{+}, the absolute minima of the AMPPES are oblate with intrinsic deformations around −7 b but for $I^{\pi}=8^{+}$ a shape transition takes place and the ground state becomes prolate with an intrinsic deformation of 10 b, the corresponding energy difference between the prolate and oblate wells amounts only to 95 keV. On the other hand, the lowest energy minima of ^{192}Pb for all spin values are always oblate.

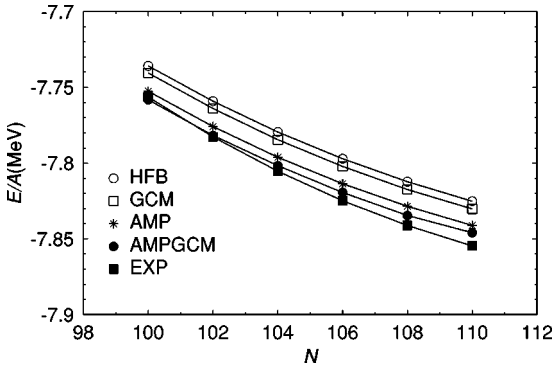

FIG. 3. Binding energies per particle as a function of the neutron number.

C. Correlations beyond the mean field: Angular momentum projected configuration mixing

From the results already described in Secs. III A and III B, we realize that not only the MFPES but also the AMPPES, for different nuclei and spin values, show the phenomenon of shape coexistence. Consequently, a configuration mixing calculation is needed for a better understanding of the structure of the states under discussion as well as to check the stability of a given minimum when quadrupole fluctuations are taken into account. With this in mind, we have carried out AMPGCM calculations along the lines described in Sec. II. The intrinsic axial quadrupole moment q_{20}, with values $-20\ \text{b} \leqslant q_{20} \leqslant 30\ \text{b}$ and with a mesh $\Delta q_{20} = 100\ \text{fm}^2$, has been chosen as generator coordinate.

The ground state energy gain, with respect to the AMP approach, by the configuration mixing amounts to −1.032 MeV, −1.081 MeV, −1.025 MeV, −1.091 MeV, −1.143 MeV, and −0.924 MeV for the nuclei $^{182-192}$Pb, respectively. One could also ask, for comparison, for the energy gain by allowing shape mixing in the wave functions in the pure GCM approximation, i.e., *without* angular momentum projection. See also Ref. [40] for further details on the calculations.[1] The energy gains, with respect to the HFB solution, are −0.819 MeV, −0.859 MeV, −0.921 MeV, −0.931 MeV, −0.959 MeV, and −0.941 MeV for the $^{182-192}$Pb nuclide, respectively. It is interesting that these numbers, though somewhat smaller, are comparable to the AMPGCM ones. In Fig. 3 we show the binding energy per

[1]The calculations shown in this paper are similar to the ones of Ref. [40], the small discrepancies in both results are due to the fact that in the results presented in this work we have included in the HFB and in the GCM calculations the term corresponding to the two body kinetic energy which was neglected in the earlier calculations.

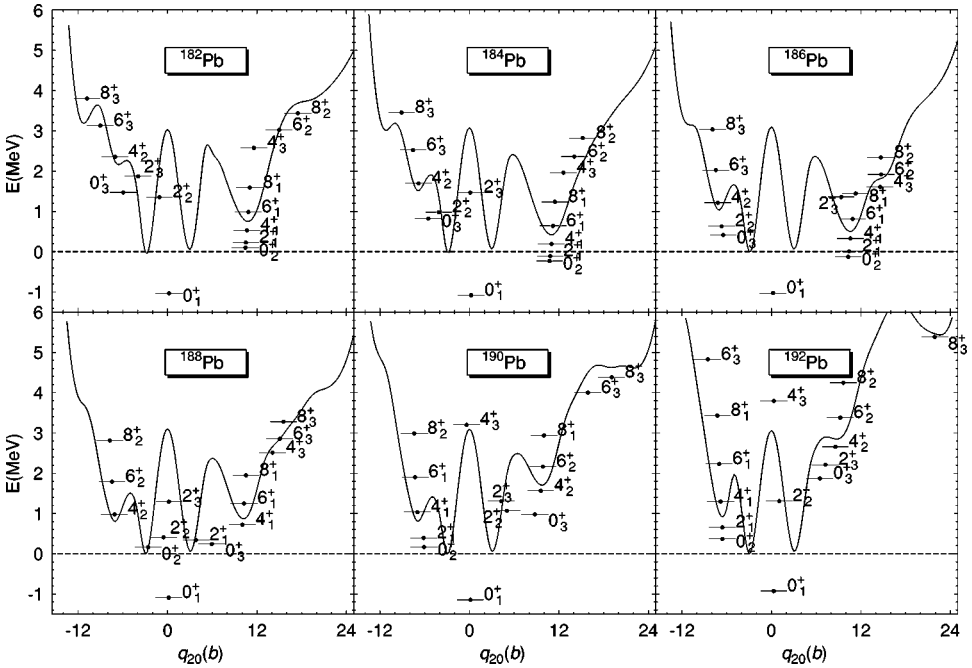

FIG. 4. Band diagrams for the nuclei $^{182-192}$Pb obtained by solving the Hill-Wheeler equation of the AMPGCM. The $I^{\pi}=0^{+}$ AMPPES is also plotted to guide the eye. See text for further details.

particle in the different approximations as well as the experimental values [59]. We find the very satisfactory results that the degree of agreement with the experiment increases with the sophistication of the theory. Notice that the largest energy gain, about 3 MeV, is provided by the AMP.

In Fig. 4 we have plotted the AMPGCM energies E^{I}_{σ}, obtained by solving the HW equation [Eq. (2)], for the ground $\sigma=1$, the first $\sigma=2$, and second $\sigma=3$ excited states in each nucleus for $I^{\pi}=0^{+}$, 2^{+}, 4^{+}, 6^{+}, and 8^{+}. Each energy level has been placed along the deformation axis according to its "average intrinsic quadrupole moment" defined as

$$\overline{q}^{I,\sigma}_{20}=\int dq_{20}|g^{I}_{\sigma}(q_{20})|^{2}q_{20}. \tag{9}$$

The values of $\overline{q}^{I,\sigma}_{20}$ are given in column 8 of Table I for the 0^{+} states and for the other spin values in Table II. In order to gain a deeper insight about the structure of the states, we have also plotted in Fig. 6 the corresponding collective wave functions squared $|g^{I}_{\sigma}(q_{20})|^{2}$ for $I=0\hbar$, $2\hbar$, $4\hbar$, and $6\hbar$.

Let us first discuss the 0^{+} states. In columns 7 and 8 of Table I the energies and intrinsic quadrupole moments of these states are given. The first noticeable fact in this table is that in the configuration mixing calculations the ground states, 0^{+}_{1}, of all nuclei are practically spherical. As we can see in Fig. 6, this is due to the fact that prolate and oblate configurations at ±3 b have almost the same weight in the 0^{+}_{1} collective wave functions. Consequently $Z=82$ remains on the average a magic proton number for these nuclei. The prolate or oblate character of the 0^{+}_{2} and 0^{+}_{3}, see Table I, is the same as in the MFA and in the AMP approaches. In fact, with the exception of the nucleus ^{188}Pb, whose quadrupole moments are only in qualitative agreement with the ones calculated in MFA and AMP, for all other isotopes the agreement of the q_{20} values obtained with the AMPGCM, AMP, and the MFA is even quantitative. Looking in Fig. 6, at the wave functions of the 0^{+}_{2} and 0^{+}_{3} states, we find that only in ^{188}Pb the corresponding wave functions have a two peak structure, this mixing being not possible either in a MFA or in the AMP approach. In the AMPGCM theory the isotope ^{188}Pb is the one where the change of the oblate and prolate character of the first excited states of the $^{182-192}$Pb isotopes takes place. It is, however, surprising that after the mixing most of the states remain rather pure: The 0^{+}_{1} states are a very specific linear combination of "cuasispherical" shapes, and with the exception of the nucleus ^{188}Pb the 0^{+}_{2} and 0^{+}_{3} are either prolate or oblate. In a situation of strong shape coexistence at the MFA one would expect, in general, strong mixing of the wave functions at a configuration mixing approach. In regard to the excitation energies and the comparison with the available experimental data we observe how the oblate minimum is pushed up in energy for the lightest isotopes and minimizes its excitation energy at a larger mass number ($A=188$) than suggested by the experiment ($A=186$) [1]. On the other hand, the prolate minimum is pushed up for the heaviest isotopes and minimizes its excitation energy for $A=184$. It is interesting to note how in ^{186}Pb, the excitation energy of the prolate minimum agrees very well with the experimental one for the corresponding 0^{+} state but, on the other hand, the excitation energy of the oblate 0^{+} state is overestimated considerably. Similar results have been obtained in Refs. [41,42].

Concerning the comparison of the different theoretical predictions for the excitation energies of the 0^{+}_{2} and 0^{+}_{3} we

TABLE II. Intrinsic and spectroscopic quadrupole moments (in e b) for $I^{\pi}=2^{+}$, 4^{+}, 6^{+}, and 8^{+} and $\sigma=1,2,3$, for the set of nuclei considered in this paper.

Nucleus	$I(\hbar)$	$\overline{q}_{20}^{I,\sigma=1}(Q_{spect}^{I,\sigma=1})$	$\overline{q}_{20}^{I,\sigma=2}(Q_{spect}^{I,\sigma=2})$	$\overline{q}_{20}^{I,\sigma=3}(Q_{spect}^{I,\sigma=3})$
182	2	10.52(−2.69)	−1.09(0.29)	−3.93(1.00)
	4	10.66(−3.49)	−7.03(2.28)	11.58(−3.78)
	6	10.84(−3.91)	14.97(−5.38)	−9.00(3.26)
	8	11.03(−4.18)	17.47(−6.64)	−10.81(4.12)
184	2	10.83(−2.75)	−4.11(1.05)	0.11(−0.03)
	4	11.00(−3.58)	−6.84(2.23)	12.60(−4.08)
	6	11.21(−3.99)	14.08(−5.02)	−7.56(2.69)
	8	11.46(−4.30)	15.20(−5.70)	−9.11(3.42)
186	2	10.41(−2.63)	−6.67(1.68)	9.36(−2.36)
	4	10.61(−3.40)	−7.16(2.28)	14.57(−4.69)
	6	10.88(−3.84)	14.73(−5.19)	−7.46(2.64)
	8	11.31(−4.20)	14.67(−5.45)	−7.90(2.94)
188	2	3.83(−0.96)	−0.53(0.13)	0.18(−0.05)
	4	10.04(−3.19)	−7.12(2.26)	14.08(−4.47)
	6	10.28(−3.59)	−7.44(2.59)	15.07(−5.23)
	8	10.52(−3.89)	−7.74(2.86)	15.57(−5.72)
190	2	−6.15(1.51)	5.01(−1.24)	4.27(−1.03)
	4	−6.97(2.19)	9.55(−3.00)	−0.38(0.14)
	6	−7.28(2.52)	9.86(−3.40)	15.87(−5.48)
	8	9.98(−3.68)	−7.42(2.70)	19.07(−6.96)
192	2	−6.58(1.62)	1.05(−0.26)	7.25(−1.79)
	4	−6.83(2.15)	8.59(−2.68)	0.32(−0.10)
	6	−7.00(2.40)	9.23(−3.15)	−8.54(2.90)
	8	−7.24(2.63)	9.66(−3.49)	21.90(−7.89)

observe in Table I that the AMPGCM values are, in general, larger than in the MFA and the AMP methods, and the agreement with the experiment deteriorates to some extent. Notice that this behavior is the opposite to the one found for the binding energy of the 0_1^+ state. To disentangle AMP effects from configuration mixing effects we can look to the pure configuration mixing calculation mentioned above, i.e., GCM *without* angular momentum projection. The quadrupole moments as well as the excitation energies of the ground states and the two lowest excited states for the nuclei $^{182-192}$Pb are presented in columns 9 and 10 of Table I. The prediction of the GCM concerning quadrupole moments reconfirm the MFA and the AMP results, i.e., the ground state are spherical and the first and second excited states are oblate or prolate depending on the nuclei. The only exceptions are the second excited states of ^{190}Pb and ^{192}Pb which in MFA and AMP are predicted to be prolate and in the GCM approach they are more spherical than deformed ones. In the GCM calculation the prolate state appears as the third excited one. With respect to the excitation energies of the prolate and oblate states we find that the GCM values are closer to the MFA and AMP results than the AMPGCM ones. The agreement with the experimental data on the average is also good. With the exception of the nuclei $^{186-188}$Pb, where there is mixing, the general trend of the GCM results as compared to the MFA is to increase the excitation energy of the 0_2^+ state and to lower the one of the 0_3^+ state, favoring in several cases the agreement with the experiment. The inclusion of the projection, i.e., the AMPGCM approach, produces a general stretching of the spectrum, and, as mentioned above, the overall agreement with the experiment is, paradoxically, not as good as the MFA, the AMP, or the GCM theory.

Often it is argued that the γ degree of freedom should be included in these type of calculations. As a matter of fact, calculations with the Gogny force by Delaroche and coworkers [39] have shown that in the neighbor Hg isotopes the triaxial shapes play an important role. To verify the effect of γ deformation in our calculations we have solved as an example the (β,γ)-constrained HFB equations for the nucleus ^{186}Pb. The corresponding energy contour plots are shown in Fig. 5. Here we can clearly see along the axial axis the three minima depicted in Fig. 1 as well as a rather soft surface in the γ direction. In fact, the triaxial barrier connecting the prolate and the oblate minima amounts to 1.25 MeV, smaller than the one connecting both minima through axial shapes (1.75 MeV). This is an indication that considering the γ degrees of freedom could change our conclusions. One should consider, however, that this is an static estimation. At the GCM level the dynamics at the (β,γ) plane should be considered and in the AMPGCM, additionally, the effect of

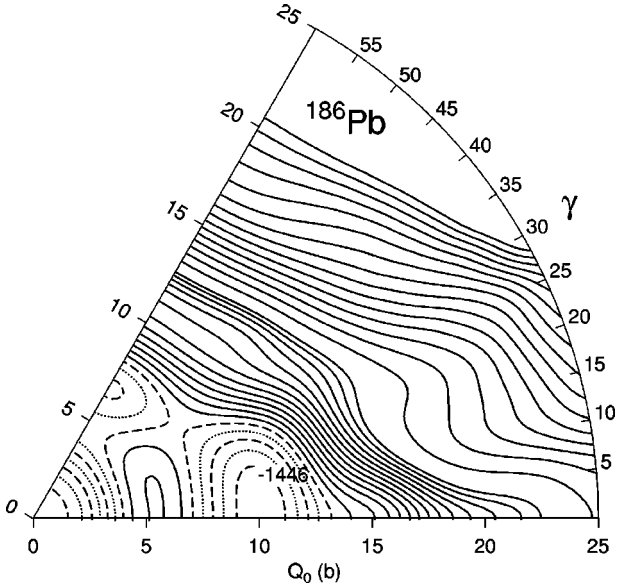

FIG. 5. Energy contour plot in the (Q_0, γ) plane for the nucleus ^{186}Pb, with $Q_0=\sqrt{q_{20}^2+q_{22}^2}$ and $\tan\gamma=q_{22}/q_{20}$. From −1446.75 MeV up to −1442.75 MeV each contour line increases by 0.25 MeV and from −1442 MeV on by 1 MeV. The contours from −1446.75 MeV up to −1445.25 MeV have been done alternating dashed and dotted lines.

the AMP will significantly change the (β,γ) energy dependence.[2] For a realistic estimation of the importance of this degree of freedom the calculations should be performed; work in this direction is in progress.

In Table II, we show the average deformations $\overline{q}_{20}^{I,\sigma}$ corresponding to the $\sigma=1,2,3$ collective wave functions of Fig. 6 for the spin values $I^\pi \geqslant 2^+$. The 2_1^+, 4_1^+, 6_1^+, and 8_1^+ collective wave functions in $^{182-186}$Pb are well inside the prolate wells. The 2_1^+ wave function in ^{188}Pb still contains a significant admixture of the oblate and prolate wells but the 4_1^+, 6_1^+, and 8_1^+ states are well prolate deformed. In ^{190}Pb, the 2_1^+, 4_1^+, and 6_1^+ collective states are well inside the oblate wells but a shape transition takes place for $I^\pi=8^+$ and the ground state becomes prolate. In ^{192}Pb, the 2_1^+, 4_1^+, 6_1^+, and 8_1^+ states are oblate. Details concerning the very interesting pattern shown by the excited states with $I^\pi \geqslant 2^+$ can also be seen from this table.

A more precise definition of the quadrupole moment for protons for each of the AMPGCM states can be obtained from the results of the exact spectroscopic quadrupole moments $Q^{spec}(I,\sigma)$ for protons (no effective charges have been used) 7. The values obtained for each of the wave functions $|\Phi_\sigma^I\rangle$ are given in Table II. We can also compute the total intrinsic quadrupole moments from the spectroscopic ones using the expression $q_{int}^{I,\sigma}=-[(2I+3)/2I](A/Z)Q^{spec}(I,\sigma)$ where the $K=0$ restriction has been taken into account and also the fact that our values of q_{20} are, by definition, half of the usual ones. The factor A/Z is used to take into account that the spectroscopic quadrupole moments are given in terms of the proton mass distribution whereas the intrinsic quadrupole moments are the total ones. As can be readily checked from Table I and II, the quadrupole moments obtained from the spectroscopic ones agree rather well with the corresponding averages $\overline{q}_{20}^{I,\sigma}$ for the spin values considered in this study.

The above mentioned results allow us to group some of the levels provided by the AMPGCM as members of bands. In the lightest isotopes $^{182-186}$Pb, the 0_2^+, 2_1^+, 4_1^+, 6_1^+, and 8_1^+ states can be considered as members of a prolate rotational band. Moreover, the $2_3^+,4_2^+,6_3^+,8_3^+$ states in ^{182}Pb and the $2_2^+,4_2^+,6_3^+,8_3^+$ in both ^{182,186}Pb are oblate and together with the 0_3^+ state could be the members of oblate deformed bands in these nuclei.

The $0_3^+,2_1^+,4_1^+,6_1^+,8_1^+$ states and the $0_2^+,2_2^+,4_2^+,6_2^+,8_2^+$ states could be associated as members of prolate and oblate bands in ^{188}Pb which show irregularities at $I^\pi=0^+$ and $I^\pi=2^+$ caused by the significant admixture of the oblate and prolate wells (see Fig. 6) in the corresponding $0_3^+,2_1^+$ and $0_2^+,2_2^+$ collective wave functions leading to a reduction of the average deformation in these states as compared with the other members of the bands.

The oblate band in ^{190}Pb has the sequence of states $0_2^+,2_1^+,4_1^+,6_1^+,8_2^+$ while the prolate band with the members $0_3^+,2_2^+,4_2^+,6_2^+,8_3^+$ shows an irregularity at $I^\pi=2^+$ which can again be traced back to the significant admixture of oblate and prolate configurations in the 2_2^+ collective wave function. The oblate and prolate bands in ^{192}Pb have the members $0_2^+,2_1^+,4_1^+,6_1^+,8_1^+$ and $0_3^+,2_3^+,4_2^+,6_2^+,8_2^+$.

The excitation energies of the predicted prolate and oblate bands are compared with the available experimental data [1–14] in Fig. 7. The excitation energies of the lowest members of the prolate bands in $^{182-186}$Pb are close to the experimental values. On the other hand, for the oblate bandhead in ^{186}Pb we have obtained an excitation energy of 1.44 MeV which largely overestimates the experimental one of 0.53 MeV. The same is also true for the oblate bandheads in $^{188-192}$Pb.

Consistent with the experimental data and also with other theoretical predictions (see, for example, Ref. [25]), the prolate bandhead dominates the structure in the lightest isotopes, minimizing with respect to the spherical ground state for $N \approx 104$. We observe that, our predictions overestimate the experimental excitation energies, i.e., our spectrum is more stretched than the experimental one. This can be traced back to many reasons: the free parameter character of our calculations or the fact that other degrees of freedom not taken into account in the calculations (triaxilities, pairing fluctuations, etc.) may play a role. A nice result is that our calculations still follow the experimental isotopic trend and support the interpretation of the experimental data in terms of shape coexisting oblate and prolate bands.

Concerning transition probabilities, very recently there have been some measurements by Dewald *et al.* [61] in ^{188}Pb. They have measured the values $B(E2,4_1^+\rightarrow 2_1^+)=160(80)$ W.u.(Weisskopf unit)—from this value they extract a deformation parameter $\beta=0.2$—and $B(E2,2_1^+\rightarrow 0_1^+)=5(3)$ W.u. In our calculations, see Fig. 4, the lowest lying 2_1^+ and 4_1^+ states have prolate deformation and the second

[2]In general, the energy gain by AMP is larger, for fixed β deformation, for triaxial shapes than for the axial ones [60].

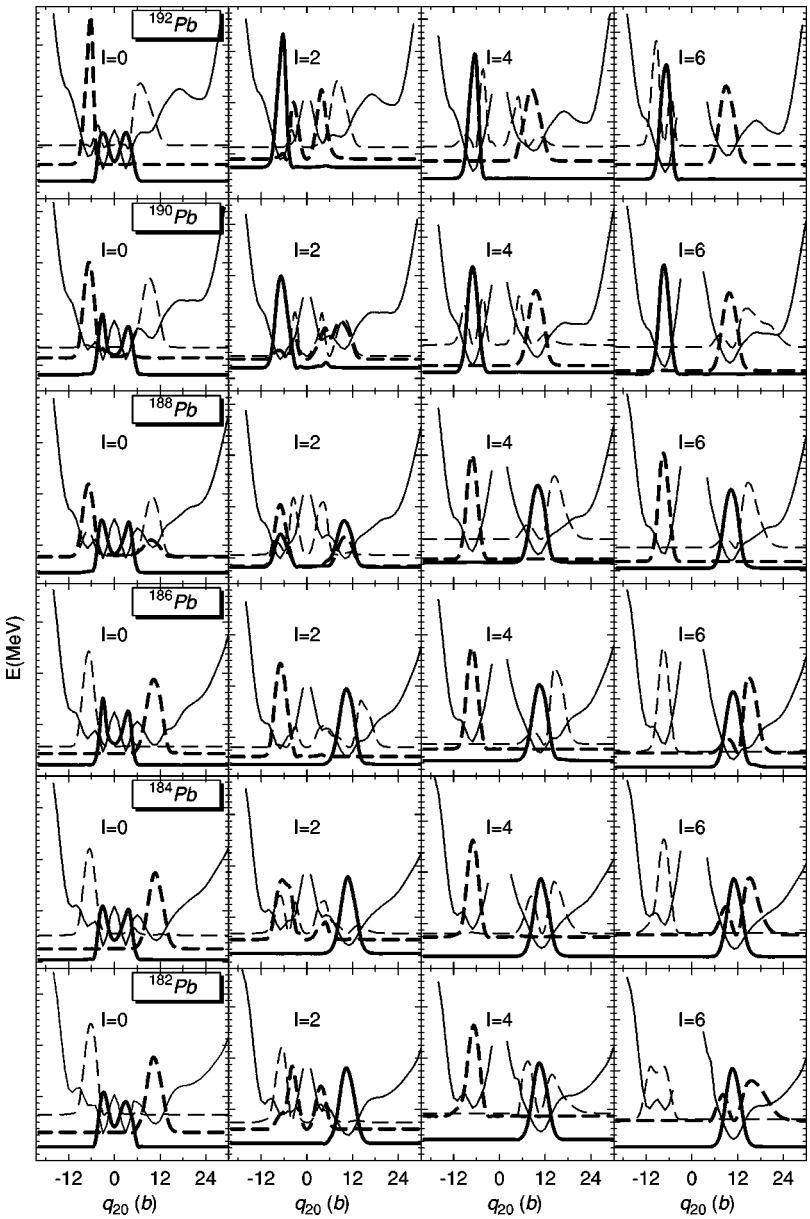

FIG. 6. Collective wave functions squared for the ground states $\sigma=1$ (continuous thick line) and first $\sigma=2$ (thick dashed line) and second $\sigma=3$ (thin dashed line) excited states of the isotopes $^{182-192}$Pb. The wave functions are given for $I^{\pi}=0^{+}$, 2^{+}, 4^{+}, and 6^{+}. The corresponding projected energy curve is also plotted for each spin value. The *y*-axix scales are in energy units and always span an energy interval of 15 MeV (minor ticks are 0.5 MeV apart). The collective wave functions have also been plotted against the energy scale after proper scaling and shifting, that is, the quantity $E^{I}_{\sigma}+15\times|g^{I}_{\sigma}(q_{20})|^{2}$ is the one actually plotted. With this choice of the scales we can read from the figure the energy gain due to quadrupole fluctuations by considering the position of the wave functions' tail relative to the projected curve.

ones, 2^{+}_{2} and 4^{+}_{2}, an oblate one. While the 2^{+} states are rather mixed and energetically close to each other, see Fig. 6, the 4^{+} ones have a clear prolate or oblate character. In our calculations we obtain $B(E2,4^{+}_{1}\rightarrow 2^{+}_{1})=262$ W.u. and $B(E2,4^{+}_{2}\rightarrow 2^{+}_{2})=142$ W.u.—the intrinsic deformations being $\beta(2^{+}_{1})=0.12$ and $\beta(4^{+}_{1})=0.28$—indicating that our 4^{+} states are not enough mixed as compared with the experimental ones. For the $E2$ transition to the ground state we obtain $B(E2,2^{+}_{1}\rightarrow 0^{+}_{1})=1.4$ W.u. and $B(E2,2^{+}_{2}\rightarrow 0^{+}_{1})=8.7$ W.u., indicating again that our wave functions are not enough mixed.

IV. CONCLUSIONS

We have performed several calculations, starting from the naive mean field approach up to the very sophisticated angular momentum projected generator coordinate method with the finite range density dependent Gogny force. The four approaches analyzed provide the same underlying basic pic-

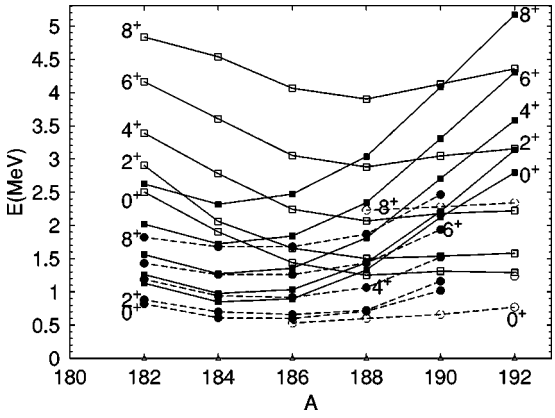

FIG. 7. Rotational bands in $^{182-192}$Pb. Prolate (oblate bands are represented by filled (empty) symbols. The circles (squares) correspond to experiment (theory). To guide the eye, states with the same spins in different nuclei have been connected with continuous (theory) dashed (experiment) lines.

ture of strong coexisting spherical, oblate, and prolate shapes.

The overall agreement with the experiment is very satisfactory, provided the free parameter character of our calculations. For the ground states energies the agreement with the experiment increases with the quality of the theoretical approximation, a quantitative agreement being only achieved in the AMPGCM. This is not the case for the excited states, where we obtain a rather stretched spectrum even in the AMPGCM. The experimental transition probabilities are in between of the theoretical predictions for prolate and oblate states. These last two facts seems to indicate that although the axially symmetric quadrupole moment seems to be the basic ingredient, it may not be sufficient and some missing correlations (triaxial deformations, pairing fluctuations, etc.) may play a role to improve the agreement with the experiment.

Of course, one should not only think about missing correlations but also keep in mind that the parameters of the force were adjusted at the mean field level. That means, a fine tuning of the force could be necessary in case that even taking into account relevant missing correlations the agreement with the experiment does not get better. We think that the three coexisting 0^+ states could be used to elucidate this point.

ACKNOWLEDGMENTS

This work was supported in part by the DGI, Ministerio de Ciencia y Tecnología (Spain) under Project No. BFM2001-0184. One of us (R.R.) would like to thank the University of Tübingen for warm hospitality during this work.

[1] R. Julin, K. Helariutta, and M. Muikku, J. Phys. G **27**, R109 (2001).
[2] J. Heese, K. H. Maier, H. Grawe, J. Grebosz, H. Kluge, W. Meczynski, M. Schramm, R. Schubart, K. Spohr, and J. Styczen, Phys. Lett. B **302**, 390 (1993).
[3] A. N. Andreyev, M. Huyse, P. Van Duppen, L. Weissman, D. Ackermann, J. Gerl, F. P. Heβberger, S. Hofmann, A. Kleinböhl, G. Münzenberg, S. Reshitko, C. Schlegel, H. Schaffner, P. Cagarda, M. Matos, S. Saro, A. Keenan, C. Moore, C. D. O'Leary, R. D. Page, M. Taylor, H. Kettunen, M. Leino, A. Lavrentiev, R. Wyss, and K. Heyde, Nature (London) **405**, 430 (2000).
[4] R. G. Allat, R. D. Page, M. Leino, T. Enqvist, K. Eskola, P. T. Greenlees, P. Jones, R. Julin, P. Kuusiniemi, W. H. Trzaska, and J. Uusitalo, Phys. Lett. B **437**, 29 (1998).
[5] P. Van Duppen, E. Coenen, K. Deneffe, M. Huyse, and J. L. Wood, Phys. Rev. C **35**, 1861 (1987).
[6] P. Van Duppen, E. Coenen, K. Deneffe, M. Huyse, and J. L. Wood, Phys. Lett. **154B**, 354 (1985).
[7] P. Dendooven, P. Decrock, M. Huyse, G. Reusen, P. Van Duppen, and J. Wauters, Phys. Lett. B **226**, 27 (1989).
[8] G. D. Dracoulis, A. P. Byrne, and A. M. Baxter, Phys. Lett. B **432**, 37 (1998).
[9] J. F. C. Cocks *et al.*, Eur. Phys. J. A **3**, 17 (1998).
[10] D. G. Jenkins *et al.*, Phys. Rev. C **62**, 021302 (2000).
[11] R. Julin, P. T. Greenlees, K. Helariutta, P. Jones, S. Juutinen, H. Kankaanpää, A. Keenan, H. Kettunen, P. Kuusiniemi, M. Leino, M. Muikku, P. Nieminen, P. Rahkila, J. Uusitalo, D. T. Joss, S. J. Joss, S. J. Willians, N-S. Kelsall, R. Wadsworth, K. Hauschild, A. Hürstel, W. Korten, Y. LeCoz, A. N. Andreyev, K. Van der Vel, C. J. Moore, C. D. O'leary, R. D. Page, M. J. Taylor, W. Reviol, and M. B. Schmith, Acta Phys. Pol. B **32**, 645 (2001).
[12] P. Van Duppen, E. Coenen, K. Deneffe, M. Huyse, K. Heyde, and P. Van Isacker, Phys. Rev. Lett. **52**, 1974 (1984) .
[13] M. Leino, R. G. Allat, J. F. C. Cocks, O. Dorvaux, K. Eskola, P. T. Greenlees, K. Helariutta, P. M. Jones, R. Julin, S. Juutinen, H. Kankaanpää, A. Keenan, H. Kettunen, P. Kuusiniemi, M. Muikku, P. Nieminen, R. D. Page, P. Rahkila, A. Savelius, W. H. Trzaska, and J. Uusitalo, Acta Phys. Pol. B **30**, 635 (1999).
[14] G. D. Dracoulis, A. P. Byrne, A. M. Baxter, P. M. Davidson, T. Kibéli, T. R. McGoram, R. A. Bark, and S. M. Mullins, Phys. Rev. C **60**, 014303 (1999) .
[15] T. Motobayashi, Y. Ikeda, Y. Ando, K. Ieki, M. Inoue, N. Iwasa, T. Kikuchi, M. Kurokawa, S. Moriya, S. Ogawa, H. Murakami, S. Shimoura, Y. Yanagisawa, T. Nakamura, Y. Watanabe, M. Ishiara, T. Teranishi, H. Okuno, and R. F. Casten, Phys. Lett. B **346**, 9 (1995).
[16] T. Radon, H. Geissel, G. Münzenberg, B. Franze, Th. Kerscher, F. Nolden, Yu. N. Novikov, Z. Patyk, C. Scheidenberger, F. Attallah, K. Beckert, T. Beha, F. Bosch, H. Eickhoff, M. Falch, Y. Fujita, M. Hausmann, F. Herfurth, H. Irnich, H. C. Jung, O. Klepper, C. Kozhuharov, Yu. A. Litinov, K. E. G. Löbner, F. Nickel, H. Reich, W. Schwab, B. Schlitt, M. Steck, K. Sümmerer, T. Winker, and H. Wollnik, Nucl. Phys. **A677**, 75 (2000).
[17] Yu. N. Novikov, F. Attallah, F. Bosch, M. Falch, H. Geissel, M. Hausmann, Th. Kerscher, H.-J. Kluge, C. Kozhuharov, Yu. A. Litinov, K. E. G. Löbner, G. Münzenberg, Z. Patyk, T. Radon, C. Scheidenberger, A. H. Wapstra, and H. Wollnik, Nucl. Phys. **A697**, 92 (2002).
[18] K. S. Toth, C. R. Bingham, J. C. Batchelder, L. T. Brown, L. F. Conticchio, C. N. Davids, R. J. Irvine, D. Seweryniak, D. M. Moltz, W. B. Walters, J. Wauters, and E. F. Zganjar, Phys. Rev. C **60**, 011302 (1999).
[19] J. F. C. Cocks *et al.*, Eur. Phys. J. A **3**, 17 (1998).
[20] N. Bijnens *et al.*, Z. Phys. A **356**, 3 (1996).
[21] A. Faessler, U. Götz, B. Slavov, and T. Ledergerber, Phys. Lett. **39B**, 579 (1972).
[22] M. Cailliau, J. Letessier, H. Flocard, and P. Quentin, Phys. Lett. **46B**, 11 (1973).
[23] F. R. May, V. V. Pashkevich, and S. Frauendorf, Phys. Lett. **68B**, 113 (1977).
[24] R. Bengtsson and W. Nazarewicz, Z. Phys. A **334**, 269 (1989).
[25] W. Nazarewicz, Phys. Lett. B **305**, 195 (1993).

[26] S. Yoshida, S. K. Patra, N. Takigawa, and C. R. Praharaj, Phys. Rev. C **50**, 1398 (1994).
[27] S. K. Patra, S. Yoshida, N. Takigawa, and C. R. Praharaj, Phys. Rev. C **50**, 1924 (1994).
[28] N. Takigawa, S. Yoshida, K. Hagino, S. K. Patra, and C. R. Praharaj, Phys. Rev. C **53**, 1038 (1996).
[29] S. Yoshida and N. Takigawa, Phys. Rev. C **55** 1255 (1997).
[30] M. Bender, T. Cornelius, G. A. Lalazissis, J. A. Maruhn, W. Nazarewicz, and P.-G. Reinhard, Eur. Phys. J. A **14**, 23 (2002).
[31] P.-G. Reinhard, M. Rufa, J. A. Maruhn, W. Greiner, and J. Friedrich, Z. Phys. A **323**, 13 (1986).
[32] M. M. Sharma, M. A. Nagarajan, and P. Ring, Phys. Lett. B **312**, 377 (1993).
[33] M. Bender, K. Rutz, P.-G. Reinhard, J. A. Maruhn, and W. Greiner, Phys. Rev. C **60**, 034304 (1999).
[34] G. A. Lalazissis, J. König, and P. Ring, Phys. Rev. C **55**, 540 (1997).
[35] T. Niksic, D. Vetranar, P. Ring, G. A Lalazissis, Phys. Rev. C **65**, 054320 (2002).
[36] N. Tajima *et al.*, Nucl. Phys. **A551**, 409 (1993).
[37] P.-H. Heenen, A. Valor, M. Bender, P. Bonche, and H. Flocard, Eur. Phys. J. A **11** 393 (2001).
[38] J. Meyer, P. Bonche, M. S. Weiss, J. Dobaczewski, H. Flocard, and P.-H. Heenen, Nucl. Phys. **A588**, 597 (1995).
[39] P. Delaroche, M. Girod, G. Bastin, I. Deloncle, F. Hannachi, J. Libert, M. G. Porquet, C. Bourgeois, D. Hojman, P. Kilcher, A. Korichi, F. Le Blanc, N. Perrin, B. Roussière, J. Sauvage, and H. Sergolle, Phys. Rev. C **50**, 2332 (1994).
[40] R. R. Chasman, J. L. Egido, and L. M. Robledo, Phys. Lett. B **513**, 325 (2001).
[41] T. Duguet, M. Bender, P. Bonche, and P.-H. Hennen, Phys. Lett. B **559**, 201 (2003).
[42] M. Bender, P. Bonche,T. Duguet, and P.-H. Hennen, Phys. Rev. C (to be published).
[43] R. Rodríguez Guzmán, J. L. Egido, and L. M. Robledo, Nucl. Phys. **709**, 201 (2002).
[44] J. Decharge and D. Gogny, Phys. Rev. C **21**, 1568 (1980).
[45] J. F. Berger, M. Girod, and D. Gogny, Nucl. Phys. **A428**, 23c (1984).
[46] R. Rodríguez Guzmán, J. L. Egido, and L. M. Robledo, Phys. Lett. B **474**, 15 (2000).
[47] R. Rodríguez Guzmán, J. L. Egido, and L. M. Robledo, Phys. Rev. C **62**, 054319 (2000).
[48] R. Rodríguez Guzmán, J. L. Egido, and L. M. Robledo, Phys. Rev. C **65**, 024304 (2002).
[49] S. Péru, M. Girod, and J. F. Berger, Eur. Phys. J. A **9**, 35 (2000).
[50] R. Rodríguez Guzmán, J. L. Egido, and L. M. Robledo, Acta Phys. Pol. B **9**, 2385 (2001).
[51] R. Rodríguez Guzmán, J. L. Egido, and L. M. Robledo, Eur. Phys. J. A **17**, 37 (2003).
[52] R. Rodríguez Guzmán, J. L. Egido, and L. M. Robledo, in *Proceedings of the International Conference on Structure of the Nucleus at the Dawn of the Century*, edited by G. C. Bonsignori, M. Bruno, A. Ventura, and D. Vretenar (World Scientific, Singapore, 2001), p. 28.
[53] J. L. Egido, L. M. Robledo, and Y. Sun, Nucl. Phys. **A560**, 253 (1993).
[54] J. L. Egido, R. Rodriguez-Guzman, and L. M. Robledo, nucl-th/0311105.
[55] L. M. Robledo, Phys. Rev. C **50**, 2874 (1994).
[56] K. Hara, A. Hayashi, and P. Ring, Nucl. Phys. **A385**, 14 (1982).
[57] P. Bonche, J. Dobaczewski, H. Flocard, P.-H. Heenen, and J. Meyer, Nucl. Phys. **A510**, 466 (1990).
[58] J. L. Egido and L. M. Robledo, in *Lecture Notes in Physics*, edited by G. Lalazissis, P. Ring, and D. Vretenar (Springer-Verlag, Heidelberg, 2003), Vol. 641, p. 237.
[59] G. Audi, O. Bersillon, J. Blachot, and H. Wapstra, Nucl. Phys. **A729**, 3 (2003).
[60] Y. Sun (private communication).
[61] A. Dewald, R. Peusquens, B. Saha, P. von Brentano, A. Fitzler, T. Klug, I. Wiedenhöver, M. P. Carpenter, A. Heinz, R. V. F. Janssens, F. G. Kondev, C. J. Lister, D. Seweryniak, K. Abu Saleem, R. Krücken, J. R. Cooper, C. J. Barton, K. Zyromski, C. W. Beausang, Z. Wang, P. Petkov, A. M. Oros-Peusquens, U. Garg, and S. Zhu, Phys. Rev. C **68**, 034314 (2003).